

# The impacts of tidal energy development and sea-level rise in the Gulf of Maine

Kresning, Boma; Hashemi, M. Reza; Neill, Simon P.; Green, Mattias; Xue, Huijie

**Energy**

*DOI:*
10.1016/j.energy.2019.115942

Published: 15/11/2019

Peer reviewed version

# The impacts of tidal energy development and sea-level rise in the Gulf of Maine

Boma Kresning[a], M Reza Hashemi*[a], Simon P. Neill[b], Mattias Green[b], Huijie Xue[c]

[a]*Department of Ocean Engineering; Graduate School of Oceanography, the University of Rhode Island, USA*
[b]*School of Ocean Sciences, Bangor University, UK*
[c]*School of Marine Science, University of Maine, USA*

## Abstract

In this study, we employed a 3-D and two-way nested Regional Ocean Modeling System (ROMS) to address several important outstanding issues regarding tidal energy development in The Gulf of Maine. We investigated the impact of projected sea-level rise (SLR) on the energy resources of the region, and examined how tidal dynamics will be influenced by energy extraction and/or SLR. Further, we assessed whether the effect of SLR on the generation of tides in the ocean (hence at the boundary of the region) is significant in these assessments. We find that the impact of SLR exceeds the impact due to energy extraction in the Gulf of Maine - even when considering very large energy extraction, of order 3.0 GW, in the Minas Passage. Although results showed that energy extraction does not significantly increase the amplitude of the tides in the far-field, a drastic change in the Bay of Fundy (e.g. full blockage) can lead to considerably higher amplitudes of tides (around 35 cm, or 12 %). As a result of 1 m SLR, the theoretical tidal energy resources in some areas, including the Bay of Fundy can increase no-

ticeably while any significant change in extracted energy highly depends on the turbine technology.
*Keywords:* Tidal energy, sea-level rise, ROMS, Gulf of Maine, Bay of Fundy, Minas Passage

## 1. Introduction

Over the last decade, tidal-stream energy development has attracted much interest in the offshore energy sector due to its predictability and lower visibility compared with offshore wind. However, due to limitations of existing technologies, it is not yet technically feasible to exploit the majority of the global tidal energy resource. Therefore, academic research and industrial research and development (R&D) have mainly focused on a few sites around the world where tidal current speeds regularly exceed 2.5 $ms^{-1}$ during a spring tidal cycle [1].

The Bay of Fundy in the Gulf of Maine (Fig. 1) is an example of a region that is feasible for tidal energy development. The free mode oscillation frequency of this bay is relatively close to that of semidiurnal lunar (M2) tidal component (the dominant tidal harmonic in the region), which leads to tidal resonance [2]. Consequently, tidal range and tidal current velocity reach extreme values in the Bay of Fundy: about 16 m in the Bay of Fundy [3] and exceeding 5 $ms^{-1}$ in Cape Sharp, Minas Passage [4], respectively. The Annapolis Tidal Power Plant has been operating in this area since 1984 with a capacity of 20MW (Fig. 1). Several research projects have been initiated in this area to test tidal energy devices. The Fundy Ocean Research Centre for Energy (FORCE) is the leading center assessing the performance of tidal

turbines operating in the Bay of Fundy. Several tidal energy devices have been tested in the FORCE site to date. For instance, Cape Sharp Tidal deployed a 2 MW tidal stream turbine in November 2016 and retrieved it in June 2017 in this site.

An ideal goal of tidal energy development is generation of electricity at a commercial scale using arrays of turbines with minimal hydro-environmental impacts. Having an extreme tidal range of 16 m, the Bay of Fundy is among a few sites around the world with such a potential. Therefore, several studies have assessed the available tidal stream resource in the Bay of Fundy (e.g. [5, 4, 6, 7, 8, 9]). In theory, it has been estimated that up to 22 kW/m$^2$ of time-averaged tidal-stream energy density, corresponding to a peak of 7 GW of total available theoretical tidal power, resides in the Minas Passage [5, 4, 10].

While the consensus among researchers is that there is minimal hydro-environment impact associated with the deployment of a single tidal energy device [11, 12, 13], there is a major concern about impacts of tidal energy extraction at larger (array) scale (e.g. [14, 15]). Consequently, several studies have investigated the impact of large-scale energy extraction in the Bay of Fundy [16, 17]. For instance, Karsten et al. [10] simulated an array of tidal-stream turbines on a 10 km grid in the Minas Passage, using the Finite-Volume Community Ocean Model (FVCOM [18]), to investigate the impact of 7.0 GW of power extraction in the Gulf of Maine. Chen et al. [18] predicted up to 15% increase in the amplitude of tides in the far-field, along the northeast coast of the US. A threshold of 2.5 GW of power extraction was suggested to avoid significant adverse effects in tidal dynamics; partic-

ularly, an increase in the amplitude of tides which leads to increased flood risk. Other researchers have also indicated that large amounts of energy extraction in Bay of Fundy (around 7 GW) will result in an increase of far-field tidal amplitudes [8].

In addition to tidal energy extraction, SLR can change the dynamics (e.g., generation and propagation) of tides in the Gulf of Maine, and globaly [19, 20, 21, 22, 23]. Wilmes [24] simulated changes in the amplitude of tidal components (M2 principal lunar semidiurnal, and K1 lunar diurnal), and amphidromic points using a global tidal model (see also Wilmes et al. [25]). Wilmes et al. [25] estimated that the M2 amplitude will increase by around 10 cm in the North Atlantic Ocean, and reduce by around 7 cm in the Indian Ocean, assuming 1 m SLR on average. Changes in the K1 component were estimated in the range of -2.5 cm to 2.5 cm, and likely to occur in coastal areas with a natural basin configuration (e.g., South East China Sea, Arafura Sea, and Sea of Okhotsk). Because tidal energy extraction and SLR can both change the dynamics of tides in the future, it is reasonable to consider them together in any impact assessments, whereas the majority of studies have ignored the effect of SLR in tidal energy resource/impact assessments (e.g., [4, 8, 5, 10, 16, 17]). However, Pelling and Green [9] considered the combined impact of SLR and power extraction of 7.1 GW in the Bay of Fundy. The simulations were performed by increasing water level scenario using a relatively simple 2-D depth averaged ocean model (which applies a relatively simple current calculation method compared to a 3-D model) with a resolution of 1-arc minute. Up to 0.5 m increase in the tidal amplitude was predicted along the US coastline in the Gulf of Maine due to tidal-stream

energy extraction in combination with 2 m SLR. Pelling and Green [9] did not include the impact of SLR on the global dynamics of tides, which affects the open boundary of the tidal model, and did not assess the impact of SLR on tidal energy resources. SLR can also impact the spatial and temporal variations of tidal energy resources. Very few studies have investigated the effects of SLR on tidal energy resources in other regions [26, 27].

As the Gulf of Maine is one of the most promising tidal energy sites in the word, in this study we employed an three-dimensional (3-D) modeling system to address a number of important unresolved issues regarding tidal energy resources and the impacts of tidal energy extraction in this region. We applied a 3-D ROMS (Regional Ocean Modeling System [28]) two-way nested (to examine far-field impacts) model, and investigated, 1) the impact of SLR on the energy resources of the Gulf of Maine, 2) how tidal dynamics will be influenced by energy extraction, and 3) if the effect of SLR on the generation of tides (at the boundary) is significant in these assessments, since it was ignored in previous studies.

## 2. Numerical model of the Gulf of Maine

### *2.1. Study area*

The study area is the Gulf of Maine, extending from 71° W to 63° W and 41° N to 46° N, covering the Scotian Shelf, Georges Bank, Jordan Basin, and the Bay of Fundy (Fig. 1). Eleven permanent tidal gauges (`tidesandcurrents.noaa.gov`) and four offshore observation buoys (`neracoos.org`) that were used for the model validation are shown in Fig. 1. Some important studies/projects regarding tidal energy development in the region

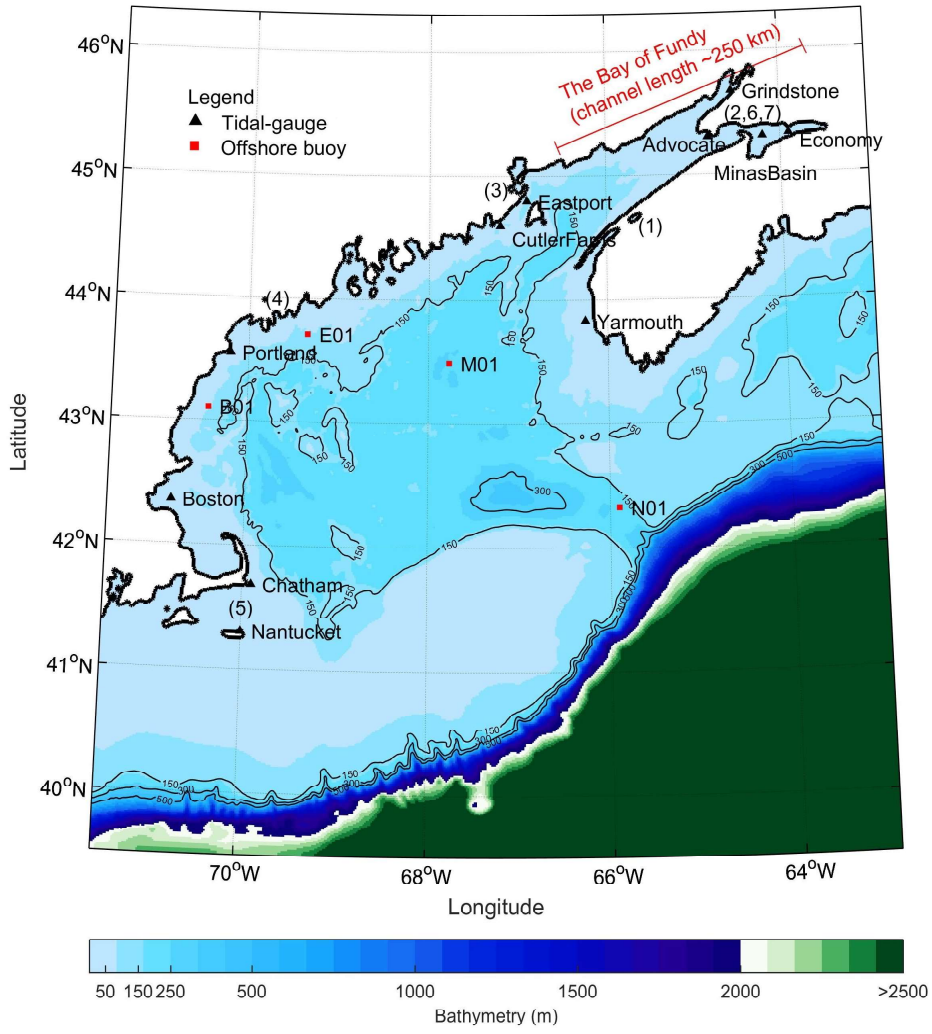


Figure 1: Map of the Gulf of Maine and its bathymetry. The red line shows the approximate length of the Bay of Fundy, black triangles denote tidal-gauges, and red squares show offshore observation buoys. The numbers show some of the sites that have been studied previously: (1) Annapolis Royal Tidal Power station [29]; (2) FORCE site; (3) Brooks [6]; (4) Brooks [7]; (5) Hagerman and Bedard [30]; (6) Cornett et al. [31]; and (7) Cornett et al. [4]

.

are also highlighted on this figure.

Tides in the Bay of Fundy are strongly semi-diurnal. It has long been known [2, 3, 32] that the significant tidal energy potential of the Bay of Fundy is due to tidal resonance. The natural oscillation period of the bay can be approximated as [33],

$$T_n = \frac{4L}{\sqrt{gh}} \tag{1}$$

where $L$ is the length of basin, $g$ is the gravity and $h$ is the depth of basin. Assuming 250 km as the length, and 50 m $\sim$ 55 m as the (mean) water depth, the natural free oscillation period will be 12.25 hr which is (considering oversimplification of Eq. 1) the period of the lunar semidiurnal tide (M2), i.e., the main component of the tide in the region. As a quick estimate, one can see that adding 3 m of water depth (e.g. due to future SLR) would reduce the period by about 30 minutes, and therefore, will change the tidal dynamics in the Gulf.

### *2.2. Tidal modeling*

To simulate the tides and tidal energy extraction, ROMS (Regional Modeling System) was applied. ROMS solves the three-dimensional Reynolds-averaged Navier Stokes (RANS) equations with hydrostatic and Boussinesq assumptions [28]. ROMS, unlike 2D depth averaged models, can capture the vertical structure of the flow and other processes such as turbulence and secondary flows [34]. The model applies a split-explicit time scheme on an Arakawa-C horizontal grid combined with terrain following (sigma) layers in the vertical. As a regional ocean model, ROMS has several capabilities in simulating ocean physics, such as tides, barotropic/baroclinic currents, and sediment transport.

*2.3. Model implementation*

ROMS has been used extensively for resource assessments and/or impact analysis of tidal energy studies around the world (e.g. [34, 35, 36]). The ROMS model of the Gulf of Maine was based on a two-way nested modeling system [37], which can increase the accuracy in the regions ofd interest with minimum additional computational cost. Two-way nesting is necessary to examine how changes in the child domain affects far-field areas in the parent grid.

A parent and a child domain with horizontal resolution of 1- and 1/3-arc minute, respectively, were created (Fig. 2). Both grids have 11 sigma layers in the vertical direction to provide sufficient details in current profile calculations. The grid construction, and other preprocesses were carried out using ROMS-AGRIF ([38]; www.croco-ocean.org). Model bathymetry was based on the 1-arc minute NOAA coastal relief model and 15 arc-second USGS bathymetric dataset for parent and child grid, respectively. To save the computational cost, wetting and drying [39] was not included in all simulations while a sensitivity analysis to this process was carried out and will be discussed later. The quadratic drag coefficient was set uniformly to 0.003. This selection was based on previous applications of ROMS at this scale (e.g., [40]) and was examined in the validation stage. For the turbulence closure model, the generic length closure model was set to the $\kappa - \epsilon$ model ($p = 3$, $m = 1.5$, and $n = -1$; [41]). Numerical time steps were set to 60 and 20 seconds for the parent and the child grid, respectively. The open ocean boundary was forced with 10 tidal constituents extracted from TPXO7 global tidal dataset (`volkov.oce.orst.edu`; [42]). Chapman and Flather

boundary conditions, were applied at the open boundary of the domain for water elevation and velocity, respectively. The tidal components included M2, S2, N2, K2, K1, O1, P1, Q1, Mf, and Mm which were used to validate the model against observed data. For simplicity, only the M2 component, which is the main tidal constituent of the region, was included in the analysis for the future scenarios (e.g., SLR and tidal energy extraction); however, for more realistic localized simulations (e.g., SLR impacts on flooding), additional tidal constituents and higher resolution models that simulate wetting and drying should be employed.

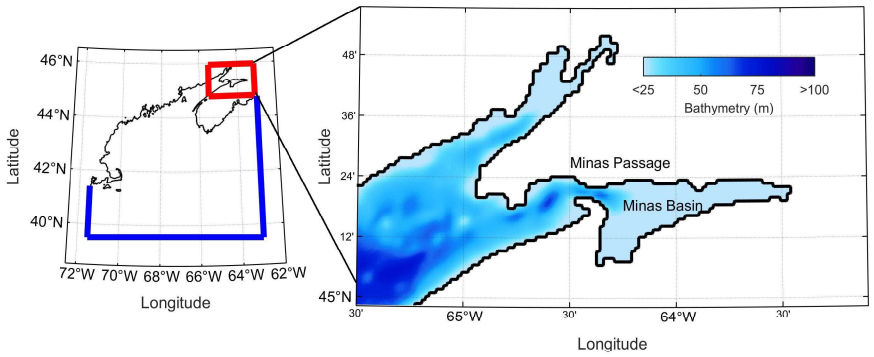


Figure 2: ROMS two-way nested domains for tidal simulations in the Gulf of Maine. The blue line shows the open ocean boundaries of the parent grid (1-minute resolution) and the red line denotes the nested 1/3 arc-minute child grid. Color scale represents the bathymetry.

To represent an array of tidal-stream turbines in the regional ocean model, we implemented a relatively simple methodology based on an additional drag coefficient [5, 14, 43, 44]. The additional drag represents the total energy loss caused by the installation of an array (i.e., extracted energy and dissipated energy in wakes etc.). Further details about the evaluation of this additional

drag is discussed in Section 3.3. There are several alternative methods to simulate turbines in regional ocean models such as quadratic Rayleigh friction [8], and 3-D representation using the actuator disc theory [45, 46]. However, because the far-field impact of tidal energy extraction was the focus of this research, simple representation of turbines as an additional sink of energy (i.e., enhanced bottom friction) seemed reasonable. Further, the energy flux before and after implementation of the tidal-stream array was calculated based on the ROMS model to make sure that the simulated energy extraction was equal to the assumed energy extraction of the array.

### *2.4. Validation*

Model results were compared with observed data at 11 water elevation gauges and 4 offshore observation buoys that are shown in Fig. 1. Because models and observed data are associated with several sources of uncertainty (e.g., model resolution, model input data, missing physical processes and simplifications in the model, and errors in measured data), discrepancies are usually expected between model results and observations. However, a model prediction should reasonably agree with the observed data within an acceptable range for error (e.g., those previously reported in other studies). For validation, the ROMS model was run for a duration of 30 days (about 1 month period is recommended by the International Electrotechnical Commission (IEC) to assess current velocity at a tidal energy site [47]). The root mean square error (RMSE) and scatter index (SI) were used to assess model performance. Lastly, bias, and mean bias error (MBE) were also calculated to determine the impacts of energy extraction and SLR with respect to the

present. The validation parameters are defined as follows:

$$\mathrm{RMSE} = \sqrt{\frac{\Sigma \left(X^{obs} - X^{sim}\right)^2}{N}} \tag{2}$$

$$\mathrm{SI} = \frac{\mathrm{RMSE}}{\overline{X^{obsv}}} \tag{3}$$

$$\mathrm{MBE} = \frac{\Sigma \left(X^{obs} - X^{sim}\right)}{N} \tag{4}$$

where $X^{obs}$ and $X^{sim}$ are observed and simulated data, respectively, and $N$ is the number of data points.

Rather than using time series, tidal harmonic analysis was carried out to estimate the tidal constituents based on the observed and modeled data. This method gives a better assessment of model performance, since tidal components are not limited to the period of simulation. Tidal analysis was performed using T_Tide MATLAB code [48]. Fig. 3 and Table 1 show the comparison of simulated and observed data for the two major semi-diurnal tidal constituents: M2 and S2. The corresponding MBE, RMSE, and SI for the M2 amplitude are 8.7 cm, 19 cm with 7%, respectively. For the M2 phase, the MBE, RMSE and SI are 4.4°, 11.8°, and 11%, respectively. The model showed a larger error for the S2 component. However, the contribution of S2 in tidal signal is much less than M2. Therefore, based on these metrics, the model performance was considered convincing, and comparable to previous numerical tidal studies in the area, which estimated about 12 cm, or 10% for the uncertainty of the M2 amplitude (e.g., [5, 49, 50, 51]).

Using the tidal current data at the observational offshore buoys, tidal ellipse parameters (which represent tidal components for velocity [48]) were calculated for the observed and the simulated depth averaged velocities at

N01, M01, B01, and E01 buoys (Fig. 1). The comparison of tidal ellipse parameters, for observed and predicted data, is shown in Table 2. Fig. 4 also provides visual comparison of tidal ellipses. As can be seen, the model performance in terms of predicting the magnitude of velocity is good. On

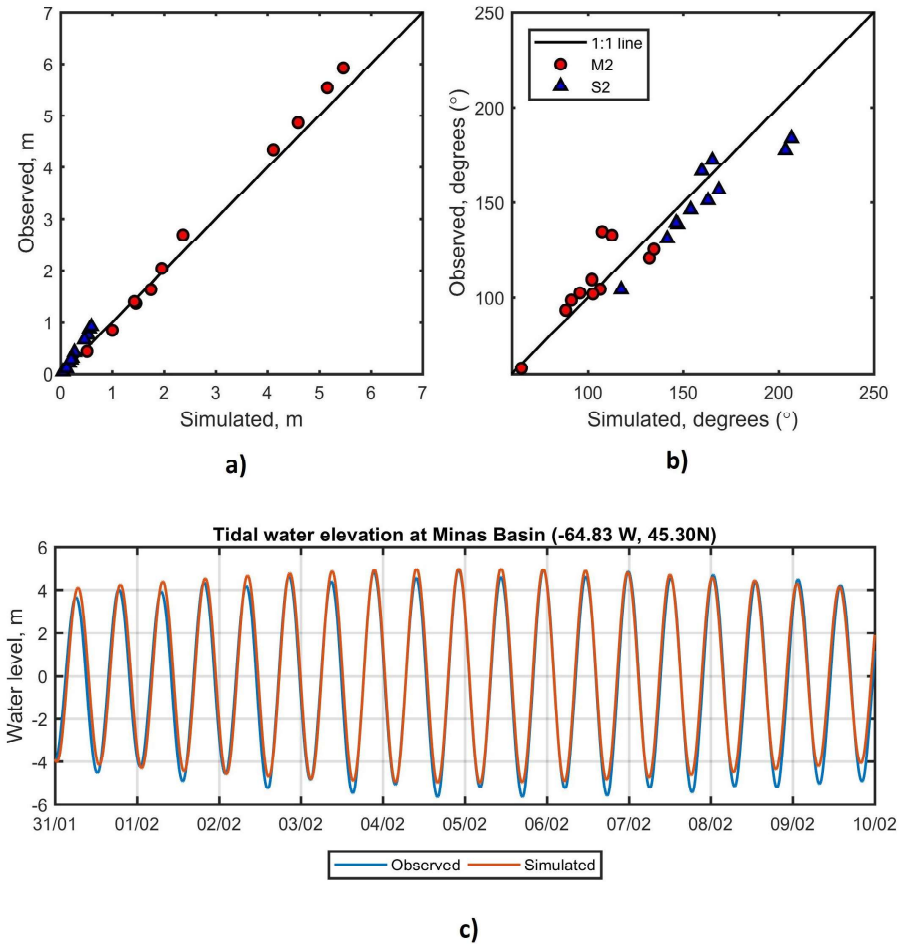


Figure 3: Comparison of tidal constituents based on observed and simulated water elevation data. Each point represents a tidal-gauge in the domain (see Fig. 1). a) Tidal amplitude, b) Tidal phase, and c) time series of water elevation at Minas Basin.

Table 1: Details of validation of model results based on the simulated tidal components.

| Constituent | Location | Observed | | Simulated | | Bias | |
|---|---|---|---|---|---|---|---|
| | | Amplitude (m) | Phase (°) | Amplitude (m) | Phase (°) | Amplitude (m) | Phase (°) |
| M2 | Portland | 1.365 | 102.500 | 1.439 | 101.729 | 0.074 | -0.771 |
| | Eastport | 2.698 | 98.700 | 2.352 | 95.917 | -0.335 | -2.783 |
| | Nantucket | 0.439 | 134.700 | 0.563 | 114.775 | 0.124 | -19.925 |
| | Boston | 1.398 | 109.400 | 1.424 | 108.108 | 0.026 | -1.293 |
| | Chatham | 0.841 | 132.800 | 0.964 | 118.929 | 0.123 | -13.871 |
| | Cutler Farris | 2.034 | 93.400 | 1.967 | 93.356 | -0.004 | 0.044 |
| | Yarmouth | 1.630 | 63.000 | 1.736 | 70.592 | 0.106 | 7.592 |
| | Grindstone | 4.860 | 104.400 | 4.646 | 111.0 | -0.214 | 6.578 |
| | Advocate Harbor | 4.340 | 102.000 | 4.170 | 106.592 | -0.170 | 4.592 |
| | Minas Basin | 5.540 | 120.800 | 5.262 | 133.345 | -0.278 | 12.545 |
| | Economy | 5.920 | 125.400 | 5.578 | 137.626 | -0.342 | 12.228 |
| | | | | | MBE | 0.087 | 4.398 |
| | | | | | RMSE | 0.199 | 11.887 |
| | | | | | SI | 7% | 11% |
| S2 | Portland | 0.206 | 138.500 | 0.229 | 157.912 | 0.023 | 19.412 |
| | Eastport | 0.420 | 139.300 | 0.371 | 156.716 | -0.049 | 17.416 |
| | Nantucket | 0.047 | 166.700 | 0.078 | 170.044 | 0.031 | 3.344 |
| | Boston | 0.213 | 146.200 | 0.227 | 164.040 | 0.014 | 17.840 |
| | Chatham | 0.109 | 172.300 | 0.151 | 177.803 | 0.042 | 5.503 |
| | Cutler Farris | 0.309 | 131.000 | 0.310 | 153.396 | 0.001 | 22.396 |
| | Yarmouth | 0.275 | 104.227 | 0.203 | 117.473 | 0.072 | -13.246 |
| | Grindstone | 0.752 | 156.023 | 0.528 | 168.707 | 0.224 | -12.683 |
| | Advocate Harbor | 0.670 | 151.391 | 0.461 | 163.036 | 0.209 | -11.645 |
| | Minas Basin | 0.860 | 176.939 | 0.558 | 203.638 | 0.302 | -26.699 |
| | Economy | 0.919 | 184.027 | 0.597 | 206.811 | 0.322 | -22.784 |
| | | | | | MBE | 0.132 | -9.746 |
| | | | | | RMSE | 0.173 | 13.810 |
| | | | | | SI | 40% | 9% |

average, the error associated with the inclination angle of the ellipse is around 7°, which is also acceptable. Nevertheless, performance of tidal models in

predicting water elevation is often better than velocity (due to higher spatial variability of the velocity field) as is the case here and elsewhere (e.g. Karsten et al. [5], Hasegawa et al. [8]).

Table 2: Comparison of tidal ellipse parameters based on the observed and predicted currents for the main tidal constituent, M2.

| Buoy | Observed | | Simulated | | Bias | |
|---|---|---|---|---|---|---|
| | Major axis (m) | Inclination angle (°) | Major axis (m) | Inclination angle (°) | Major axis (m) | Inclination angle (°) |
| N01 | 0.429 | 151.330 | 0.533 | 140.532 | -0.104 | 10.798 |
| M01 | 0.211 | 95.545 | 0.205 | 92.860 | 0.006 | 2.685 |
| B01 | 0.048 | 120.483 | 0.059 | 122.408 | -0.011 | -1.925 |
| E01 | 0.053 | 68.643 | 0.083 | 78.145 | -0.031 | -9.502 |
| | | | | MBE | -0.035 | 0.514 |
| | | | | RMSE | 0.054 | 7.379 |
| | | | | SI | 29% | 7% |

## 3. Results

Through the application of the ROMS model, tidal dynamics and tidal energy resources in the Gulf of Maine will be presented first. The impact of SLR on tidal energy resources, and the effect of tidal energy extraction (combined with SLR) on the dynamics of tides will be discussed, subsequently. Some factors such as the significance of SLR on generation of tides (e.g. boundary forcing) that were ignored in previous studies will be considered in more detail. For simplicity, we limited these discussions to the M2 tidal constituent which is the major component of the tidal energy resources in the Gulf of Maine, similar to previous research (e.g. [5, 8, 9, 31]).

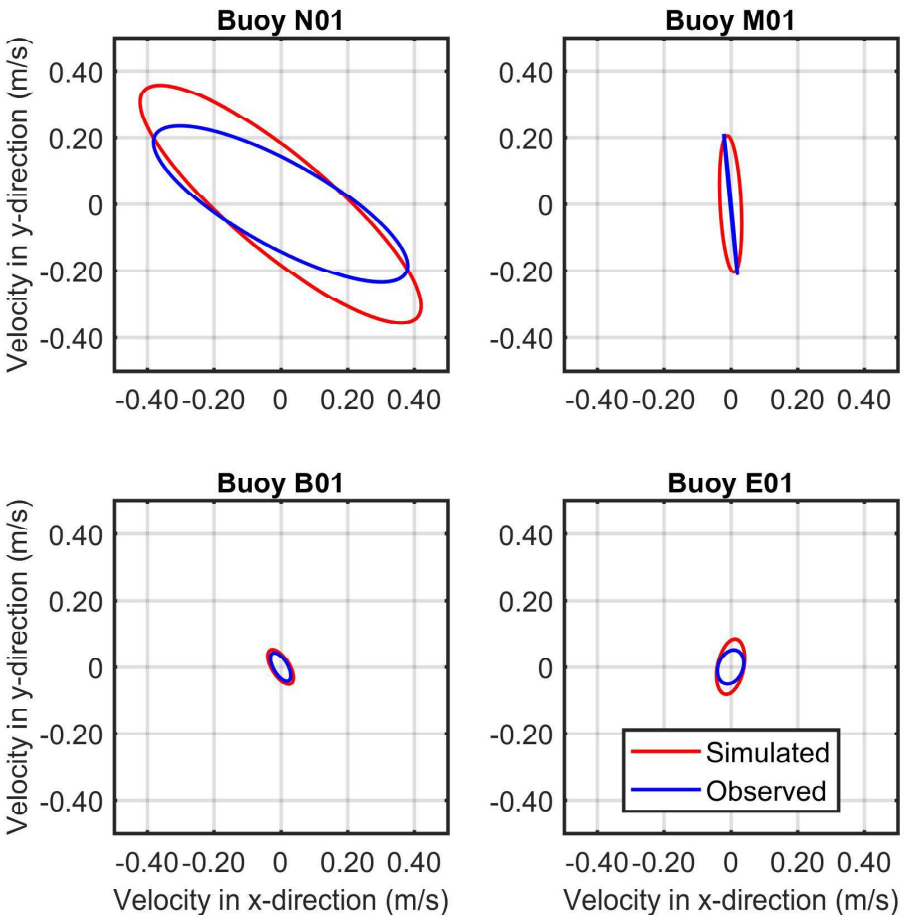


Figure 4: Comparison of simulated M2 tidal ellipses with those from observed data (see Fig. 1 for buoy locations).

### *3.1. Present Tides in the Gulf of Maine*

A classical way to represent the dynamics of tides in a region is using co-tidal charts, for water elevation, and tidal ellipses for tidal currents (e.g. see Pingree and Griffiths [52]). The T_Tide MATLAB code was used to analyze the time series of water elevation and current velocities throughout the

computational domain. Using tidal constituents and tidal ellipse parameters, co-tidal charts and tidal ellipse maps were generated; see Figs. 5 and 6 for the present (baseline) scenario. The results can be compared with those from previous studies (e.g. [8]), which show a similar pattern. High current velocities ($> 1.5\,\mathrm{ms}^{-1}$) can be seen in several regions including Nantucket, around the continental slope of the Gulf of Maine, Grand Manan Island, the western side of Nova Scotia, and Minas Passage. Tidal ellipses are almost rectilinear in the Bay of Fundy, which is an important characteristic for tidal energy extraction.

### *3.2. Effect of sea-level rise on tidal energy resources*

Tidal energy density was computed as an indicator of the theoretical tidal energy resource:

$$P_t = \frac{1}{2}\rho u^3 \tag{5}$$

where $P_t$ is the hydro-kinetic energy density, $\rho$ is the water density, and $u$ is tidal current speed. $P_t$ shows the average hydro-kinetic energy of tides per unit square of a turbine swept area, assuming that 100% of the energy is converted. The maximum efficiency of tidal turbines vary (e.g., around 45% was reported for a Marine Current Turbine device [54]). The peak value of tidal energy density was estimated to be 72 $\mathrm{kW/m^2}$ during the spring tide in Minas Passage (see [31] as a comparison), which is substantially larger compared with other locations in the Gulf of Maine (less than 5 $\mathrm{kW/m^2}$), because the power density is proportional to the cube of the velocity. The time-averaged tidal energy density (for 30 days of simulation time) is another indicator of tidal energy resources. For 'technical' tidal resource assessments,

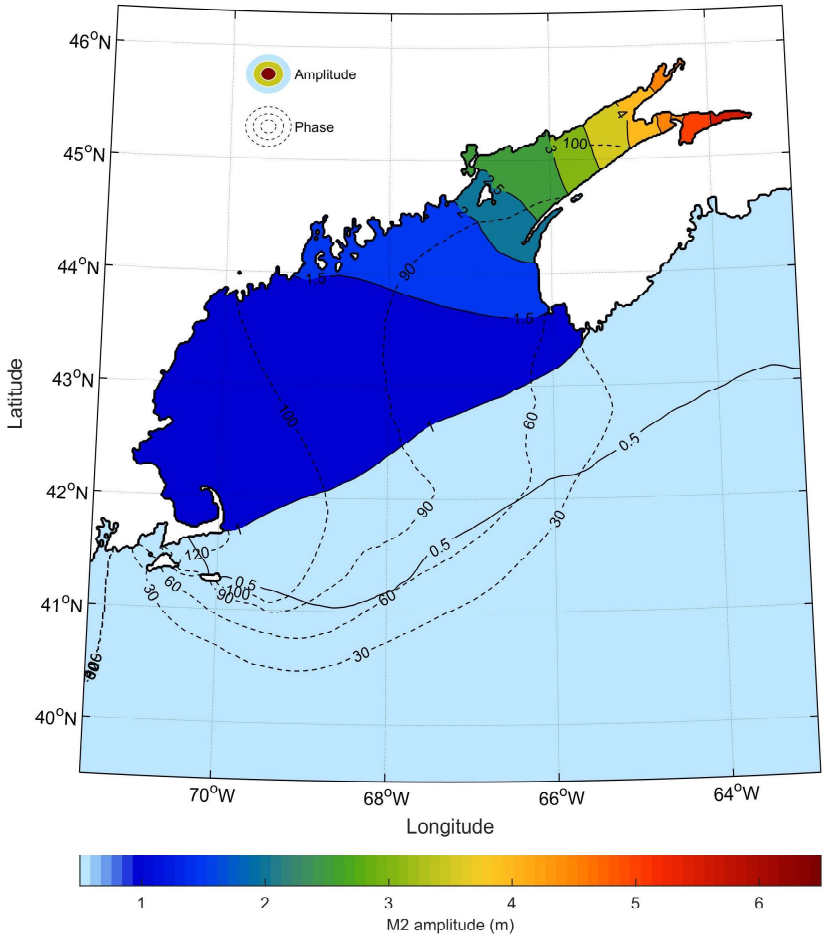


Figure 5: M2 co-tidal chart of the Gulf of Maine. Color scale denotes the amplitude of M2 constituent and dashed lines represent the corresponding tidal phase contours. Absence of co-tidal (phase) lines in the Bay of Fundy is indicative of a standing wave system [53].

however, the cut-in speed and efficiency of a turbine lead to a larger difference between the theoretical and the technical resource because "first generation" tidal energy turbines cannot efficiently generate electricity at tidal current speeds $< 1$ ms$^{-1}$[1, 55]. Nevertheless, we used the theoretical energy to avoid

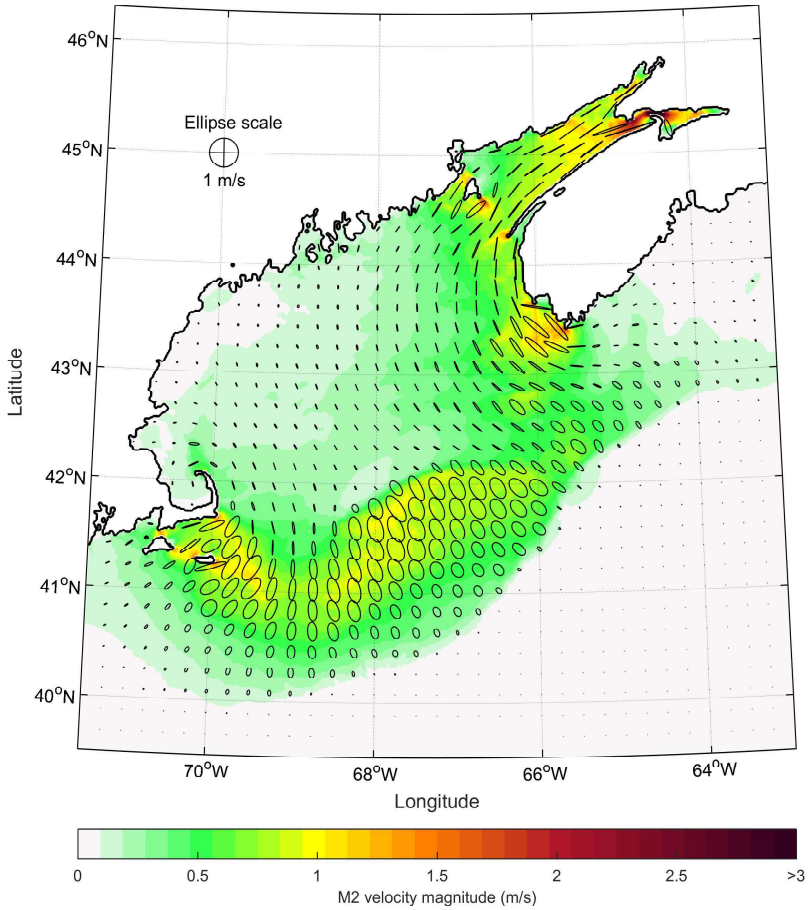


Figure 6: M2 tidal ellipse map of the Gulf of Maine. Color scale represents the peak of maximum tidal currents, and the ellipses are represented by black lines.

limiting the analysis to any specific turbine technology. The time-averaged energy density over the Minas Passage (spatially averaged) was calculated as 14.4 kW/m$^2$.

The effects of SLR on the tidal energy resource was simulated by modi-

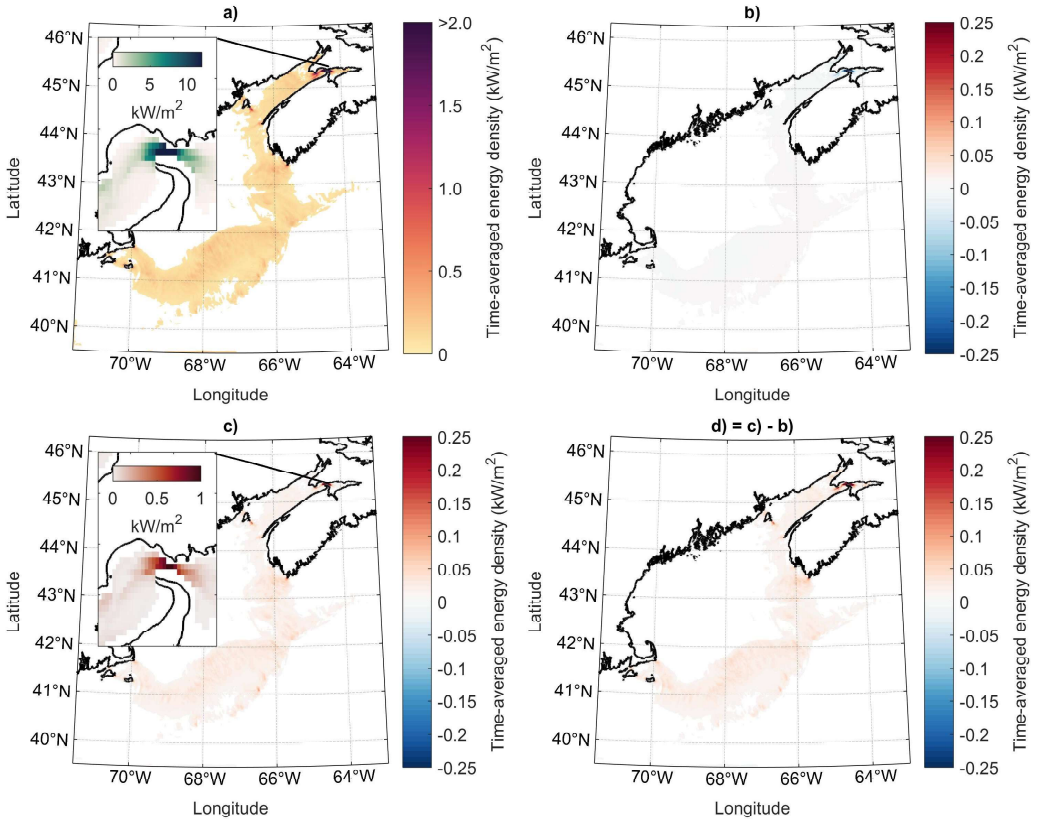


Figure 7: The tidal energy density in the Gulf of Maine: a) Present resource; b) Change in the available resources due to 1 m increase in bathymetry; c) Change in the available resources due to change of bathymetry and the corresponding forcing at the boundary; d) Difference between c and b.

fying both water depth (bathymetry) and the boundary forcing of the tidal model. Since SLR affects global tidal dynamics, it will change tidal components at the boundary of the domain, and consequently open boundary condition. According to a recent study by NOAA [56], sea level in 2050 will rise in the range of 0.45 m to 1.03 m in the Gulf of Maine assuming an intermediate to an extreme scenario, respectively. Fig. 8 shows the high and

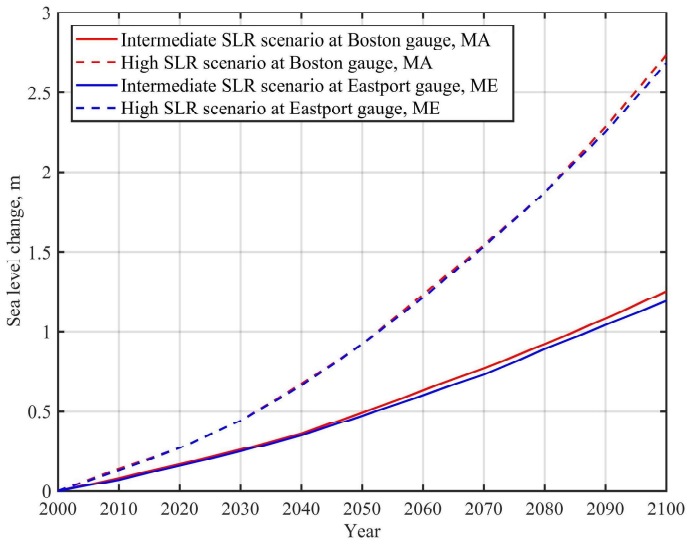


Figure 8: Intermediate and high SLR scenarios at Boston and Easport gauges [56].

the intermediate SLR scenarios at Boston and Eastport gauges. Assuming the intermediate scenario, sea level will rise by 1.02 m by 2090 in this area. Therefore, a 1 m SLR was assumed as a likely scenario for this assessment. The water depth was uniformly increased by 1 m assuming a negligible change in the shape of the basin, e.g. due to sediment distribution or changes in the coastline. To account for the change in the amplitude of tidal components at the boundary, we used tidal constituent information produced for Wilmes [24] interpolated to the present model boundary. It is true that SLR may not be uniform over the domain. Wilmes [24] show, using 5 -12m SLR (5 m for a West Antarctic collapse and 7m for a Greenland collapse) that the response in the Gulf of Maine is relatively insensitive to these changes along the boundary. For simplicity, we therefore use the uniform case here.

Fig. 7 shows the impact of SLR on the tidal energy resources. The im-

pact is more significant when the change in the forcing at the boundary is implemented (Fig. 7 c) while no significant change is observed if only water depth was changed (Fig. 7b). Generally, SLR leads to an increase in the theoretical tidal energy resource (due to propagation of more tidal energy from the ocean to the Gulf of Main), particularly in the Minas Passage (around 0.81 kW/m2). This increase was estimated based on the tidal energy density, and regardless of the size of an array or the performance of turbines. Alternatively, Annual Energy Production (AEP), for a more realistic analysis, can be evaluated by combining the time series of velocity over a year and a power curve (see, for instance, IEC 62600-201 standard for tidal energy characterization). For example, if a 1.2 MW SeaGen turbine is deployed in Minas Passage, the mean AEP of the single turbine will be around 7.10 GWh (assuming energy extraction in both ebb and flood currents and no cut-out speed) with no SLR. The SeaGen 1.2 MW turbine has a published curve with a cut-in speed of about 1 m/s and rated output speed of about 2.5 m/s [57, 34]. Adding 1 SLR, leads to an increase tidal energy, and AEP of 7.2 GWh which is not a significant increase. This is because any increase in the current velocity above the rated output speed (i.e., 2.5 m/s here) does not lead to more power generation since the power remains constant in this range of velocity (e.g., 1.2 MW for this example). Therefore, any increase in extracted power due to SLR is highly dependent on the turbine technology and the current speed range at a particular site of interest.

### *3.3. The impact of SLR combined with tidal energy extraction on the Gulf of Maine*

As mentioned earlier, because we intended to assess the far-field and regional impacts of tidal energy extraction in the Minas Passage, we used a relatively simple methodology that represented energy extraction as additional drag or friction in the model. The additional drag coefficient introduced by turbines can be estimated as,

$$\overline{P} = \frac{\int_t F_D u dt}{T} = \frac{\int (\rho C_d^* u|u| A_h) u dt}{T} = \rho C_d^* A_h \frac{\int |u|^3 dt}{T} = \rho C_d^* A_h \overline{|u|^3} \qquad (6)$$

where $\overline{P}$ is the time averaged energy loss in a grid cell due to tidal energy extraction, $u$ is the depth averaged velocity, $F_D$ is additional bottom drag force representing a tidal energy energy array (i.e., useful energy extraction and dissipation caused by turbine wakes etc.), $T$ is the period of a tidal cycle, $A_h$ is the area of a cell that is covered by turbines in the model, and $C_d^*$ is the additional drag coefficient [21]. The additional drag where turbines are installed was added to the 54 cells where the turbines would be located (see Fig 9b). As the velocity before and after increasing the drag will change, a reliable method is to apply the additional drag iteratively: 1) estimating an additional drag coefficient based on Eq. 6 using undisturbed current averages; 2) examining the tidal energy flux before and after the enhancement of the drag using each cell; 3) estimating the difference of energy flux, before and after power extraction, as an indicator of the extracted power. The area which was considered for the tidal array site in Minas Passage is shown in Fig. 9 (a similar area was considered in other studies [4, 5, 8, 9]). Based on the simulations, the time-averaged theoretical tidal energy density over this

area is 19.9 kW/m$^2$ (see also Cornett et al. [4]). Using this simple method, an additional drag coefficient of 0.0063 over 10 km$^2$ horizontal area in Minas Passage (Fig. 9) was considered. The enhanced drag coefficient of 0.0093 was applied to the area covered by turbines. Consequently, the average tidal energy flux (averaged over the cells and over time) reduces by around 3.0 GW. We should emphasize that this 3.0 GW energy loss does not necessarily indicate the capacity of a tidal array; instead it represents the maximum possible tidal energy loss in the development area. Many assumptions with regard to the type of turbines, capacity factor, and power curve should be made to compute the size of an array which leads to 3.0 GW time averaged energy loss. Several other studies have considered 2.5 GW energy extraction for their impact assessments [8, 10, 21].

Fig. 10 shows the contour lines of the change in tidal amplitude due to energy extraction. Extraction of 3.0 GW results in around 1.0 cm to 1.5 cm increase in far-field areas along the US coastline, and a reduction of 5 cm in the Bay of Fundy.

The next question is whether SLR can significantly change the response of the Gulf of Maine to tidal energy extraction. To address this question, 1 m SLR, in addition to tidal energy extraction, was concurrently implemented in the simulations, and we compare tidal amplitudes in the Gulf with and without energy extraction. According to the results (Fig. 11), the combined impacts of tidal energy extraction leads to a 5 cm increase in tidal amplitude in the far-field, covering the coastline of US and Canada, but the majority of this change (around 4 cm) is due to SLR. Therefore, the impact of SLR on tidal dynamics in the Gulf of Maine, particularly around the US coastline,

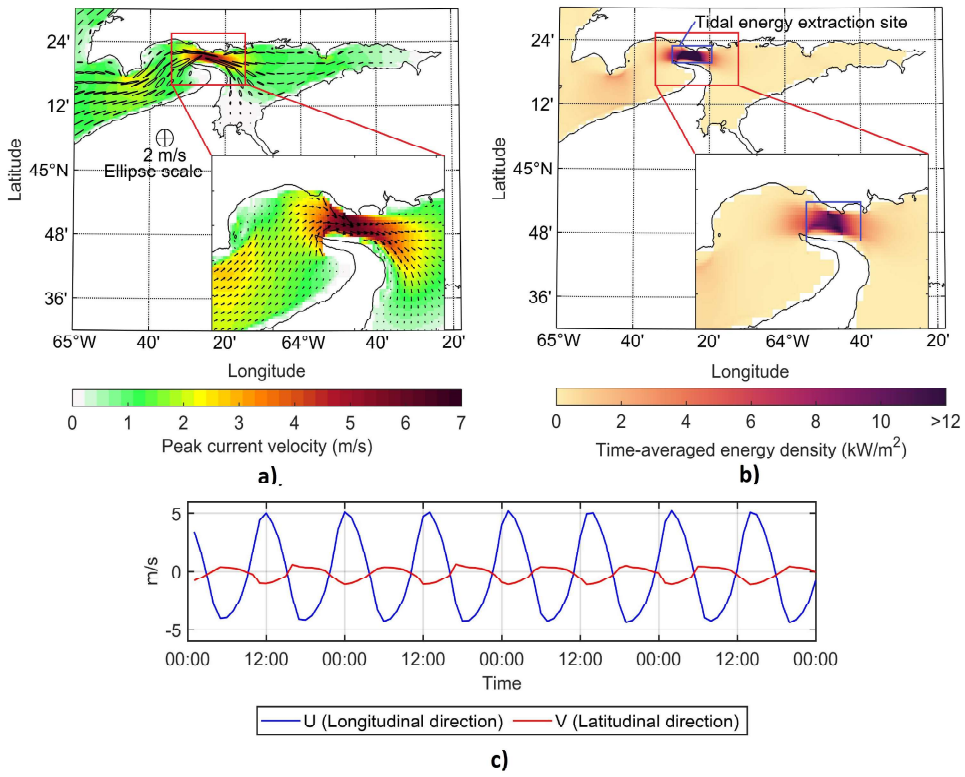


Figure 9: Tidal energy resources in Minas Passage. a) Peak current speed and tidal ellipse; b) Time-averaged energy density over spring-neap cycle; c) Time series of U and V component of tidal current velocity in Minas Passage.

significantly exceeds the contribution from large scale tidal energy conversion.

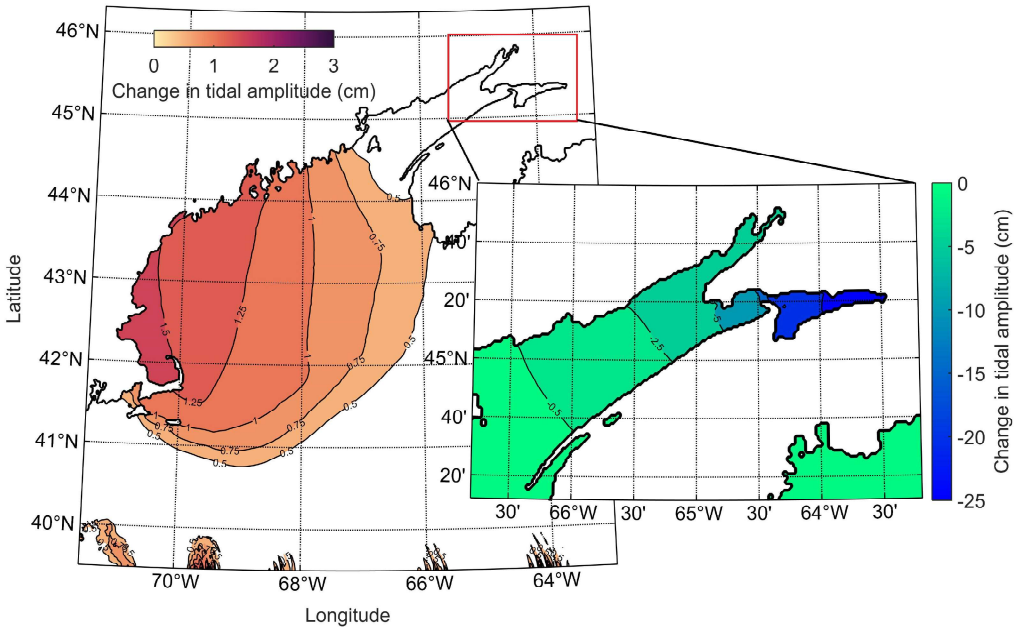


Figure 10: Impacts of 3.0 GW energy extraction in the Gulf of Maine. Positive and negative changes are represented in the left and right panel, respectively.

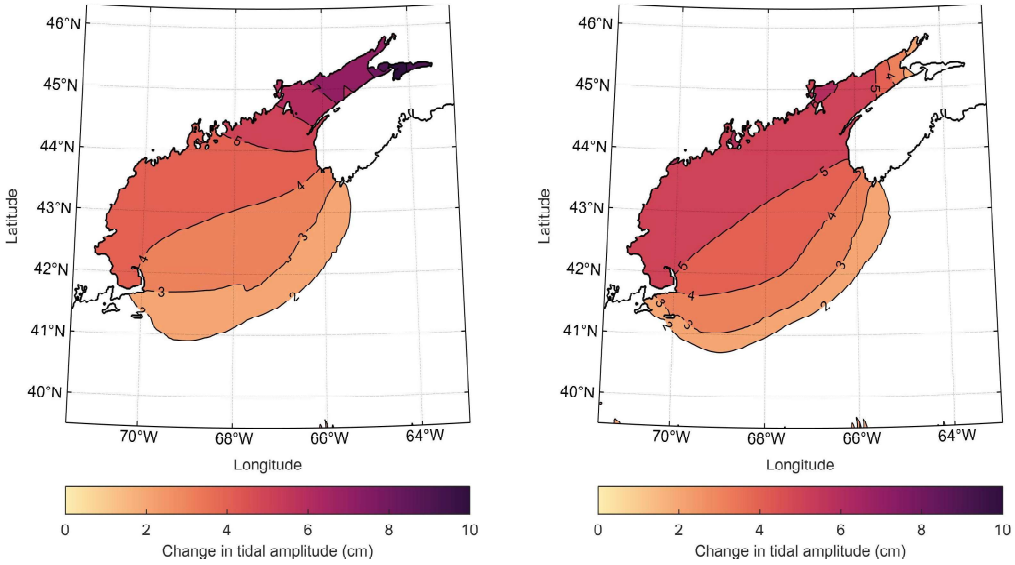


Figure 11: Changes in M2 tidal amplitude due to SLR and energy extraction scenarios; a) only due to 1 m SLR and b) due to 3.0 GW power extraction in Minas Passage combined with 1 m SLR.

## 4. Discussion

We showed that tidal energy extraction in the Gulf of Maine does not significantly increase the amplitude of tides in far-field areas such as along the neighboring US coastlines of Massachusetts, New Hampshire and Maine. However, it can be shown that the tidal dynamics in the Gulf of Maine are sensitive to the Bay of Fundy if the flow regime in the Bay is changed drastically. As an extreme case, we investigated total blockage of the Bay to conceptually examine the impact of the Bay on the far-field tides. Fig. 12 and Table 3 show the results, which indicate a significant increase (35 cm) in tidal amplitude along the US coastline, which would have negative consequences in terms of flooding. Therefore, tidal stream development would have far less impact on far-field areas, in contrast to tidal barrages.

We used a two-way nested model (1 minute resolution in the Gulf of Maine and 1/3 minute resolution in the nested domain) to increase the accuracy of the model in the Bay of Fundy. To investigate the importance of nesting, we also ran a single grid model (parent grid covering the whole domain and compared the results with the nested model. The results (which are not shown for brevity) indicated that nesting does not significantly affect/improve the simulations in the areas far from the Bay of Fundy in the Gulf of Maine. The two-way nesting however improves the simulations in the Bay itself, providing better accuracy in currents calculation that is important for tidal stream array positioning, and therefore is a preferred method to implement ROMS model in similar studies. Further, as changes outside the child domain are of interest, a two-way nested model should be implemented.

Wetting and drying was not included in simulations to reduce the com-

putational cost. Whereas including wetting and drying is important in the study of SLR impacts on coastal flooding at local scales, this study was focused on regional impacts of tidal energy extraction and SLR in the Gulf of Maine. Further, a sensitivity analysis was carried out and indicated no significant change in the results, particularly in stations shown in Fig. 1. The results of this sensitivity analysis was not shown for the sake of brevity.

Many marine current turbines have a cut-in speed of between 1 $ms^{-1}$ to 1.5 $ms^{-1}$ [55]. Therefore, suitable sites for tidal energy development require a peak (spring) current velocity of at least 2.5 $ms^{-1}$ in water depths of 25 m to 50 m. Also, for future generations of tidal stream devices, peak velocity of 2.0 $ms^{-1}$ has been discussed in the literature [1]. Based on these criteria several locations in the region have a potential for tidal energy development. In addition to the Minas Passage with a peak spring velocity of 6.0 $ms^{-1}$, other potential sites include Grand Manan Island, Nantucket, Westport, Big Tusket Island, and Shag Harbor.

In this research, energy extraction was simulated by enhancing the bottom drag coefficient. This method was used as it is relatively simple, is associated with low computational cost, and is suitable for examining the impact of energy extraction in the far-field. Other methods, which are more complex, require higher grid resolution, and could be implemented if the flow field in the vicinity of the array is of interest [46, 45]. In IEC Technical Specification 201 [47], both methods are recommended for modeling tidal resource characterization. These methods simulate a turbine in the water column (3-D) as a sink/source in the momentum and turbulence equations, and require much finer resolution (e.g. 20 m), which leads to much larger computational

cost.

Results of this study showed that the combined impact of tidal energy extraction and SLR is nonlinear to some extent. However, linear superposition of the impacts will lead to similar outcomes. For instance, in the Minas Passage, 1 m SLR leads to a 10.9 cm increase in the amplitude of M2. Tidal energy extraction at the scale of 3.0 GW leads to 13.5 cm decrease, separately. Linear superposition of these impacts leads to 2.6 cm reduction in the tidal amplitude. The nonlinear simulation results in 2 cm decrease in amplitude, i.e. a relatively similar result, and one that would allow a larger number of scenarios to be explored for the same computational cost.

Table 3: Summary of the impact study at selected locations in the Gulf of Maine

| | Calculated tidal amplitude from model scenarios (cm) | | | | |
|---|---|---|---|---|---|
| Location | Present | Blockage | 2.5 GW | 1 m SLR | 1 m SLR + 3.0 GW |
| Boston, MA | 142.3 | 182.0 | 143.9 | 146.7 | 148.1 |
| Portland, ME | 146.2 | 185.2 | 147.7 | 150.9 | 152.2 |
| Minas Passage | 486.1 | - | 472.5 | 497.0 | 484.1 |
| | | | Difference (cm) | | |
| Boston, MA | - | +30.0 | +1.6 | +4.4 | +5.8 |
| Portland, ME | - | +39.0 | +1.5 | +4.7 | +6.0 |
| Minas Passage | - | - | -13.5 | +10.9 | -2.0 |

The impacts of tidal energy extraction on sediment transport has been discussed in several research [58, 59, 16, 14]). Depending on the size of array and other factors (e.g., tidal asymmetry) the impact can be significant. Therefore, further research is necessary to investigate the combined impacts of tidal energy extraction and SLR on sediment transport in this region.

Model uncertainty has an important role in the analysis that was presented here. In addition to the magnitude of SLR, there is always a dis-

crepancy between model results and observations. In addition to model uncertainty (due to input/forcing data [e.g., bathymetry, friction coefficient] and model simplifications), observed data are also subjected to measurement errors. Results of this study provide an insight into the magnitude and direction of the changes due to SLR and/or tidal energy extraction in the Gulf of Maine. While uncertainties can change the absolute values of the results (e.g., tidal energy density at a site), our sensitivity analysis showed that the direction and magnitude of the impact (i.e., relative changes in values) does not vary within the range of uncertainties in the simulations.

## 5. Conclusion

In this study, the combined impact of tidal energy extraction and SLR on the tidal dynamics of the Gulf of Maine was investigated using a 2-way nested ROMS model. Simulation results demonstrated sensitivity of tidal dynamics in the Gulf of Maine to flow disturbances in the Bay of Fundy. In general, it was shown that the impact of SLR is much greater than the impact of tidal energy extraction in the Bay of Fundy - even when considering a very large tidal array of order 3.0 GW in the Minas Passage.

In order to investigate the effect of SLR on the dynamics of the tides in the Gulf of Maine, it is important to consider the change in the amplitude of the tides at the boundary (e.g., Continental Shelf Slope), as well as changes in the bathymetry of the domain. Considering only changes in the bathymetry leads to inaccurate results.

SLR is expected to increase the 'theoretical' tidal energy resources in the areas of interest in the Gulf of Maine due to propagation of more tidal

energy from the ocean to the Gulf of Maine. However, increase in extracted power or 'technical' energy resource due to SLR is highly dependent on the turbine technology and the current speed range at a particular site of interest. Despite this possible slight gain in tidal energy resources, negative impacts of SLR such as increase in flooding and coastal erosion should be considered in a comprehensive assessment of SLR impacts in this region [60].

Although numerical simulations showed that tidal energy extraction does not significantly increase the amplitude of the tides in far-field regions, particularly along the neighboring US coastlines, a drastic change in the Bay of Fundy (e.g. full blockage) will lead to considerably higher tidal amplitudes (around 35 cm). This shows that tidal stream energy development in general is preferred compared with other methods such as tidal barrages or lagoons, as has been recommended in other studies (e.g. [4]).

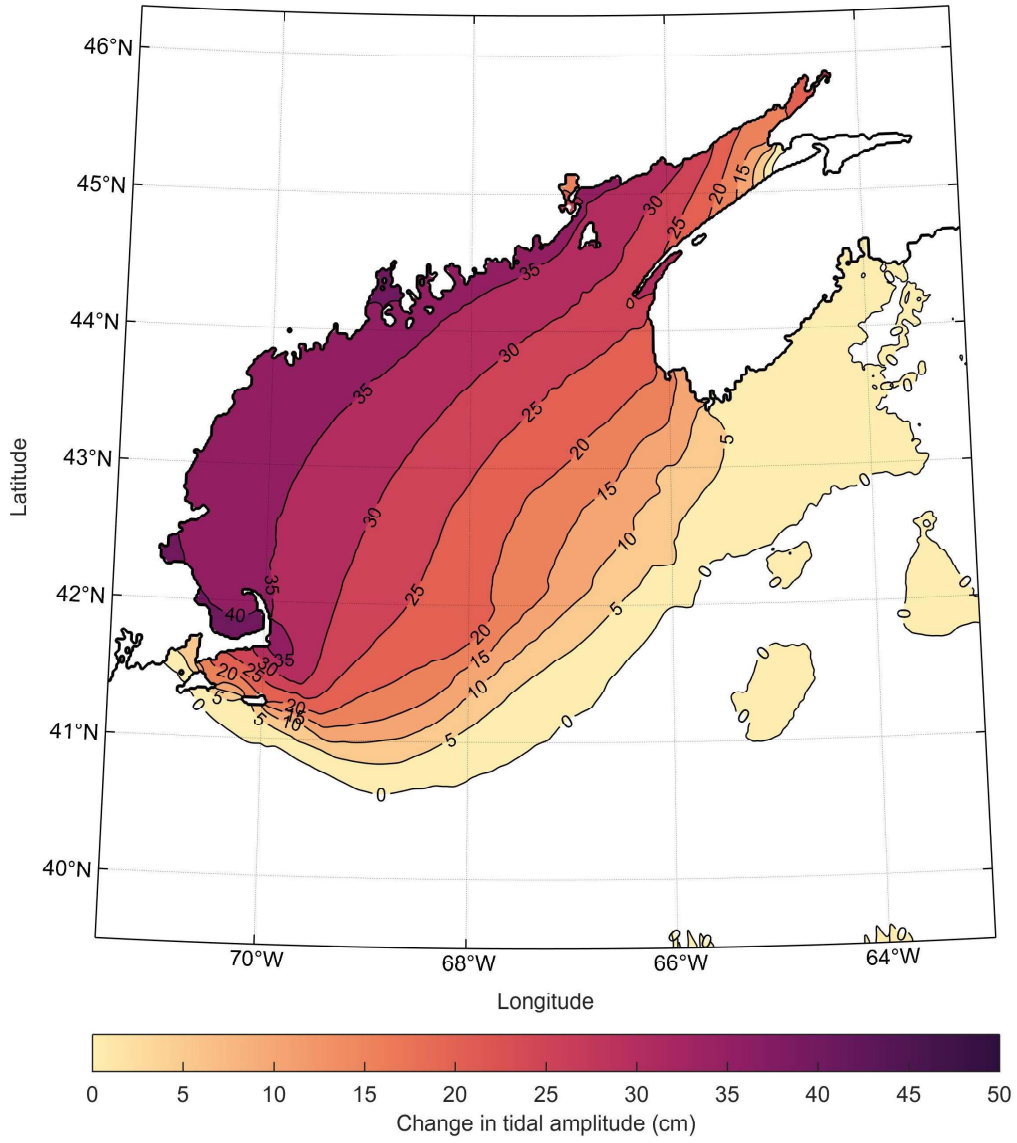


Figure 12: Impacts of the total blockage (e.g. a barrage) of Minas Passage, on M2 tidal amplitude.

**Acknowledgment**

The authors would like to thank Ministry of Marine Affairs and Fisheries, Indonesia for supporting PhD studies of Boma Kresning.

**References**

[1] Lewis M, Neill S, Robins P, Hashemi M. Resource assessment for future generations of tidal-stream energy arrays. Energy 2015;83:403–15.

[2] Garrett C. Tidal resonance in the Bay of Fundy and Gulf of Maine. Nature 1972;238:441–3.

[3] Greenberg DA. Modeling tidal power. Scientific American 1987;257:128–31.

[4] Cornett A, Cousineau J, Nistor I. Assessment of hydrodynamic impacts from tidal power lagoons in the Bay of Fundy. International Journal of Marine Energy 2013;1:33–54.

[5] Karsten RH, McMillan J, Lickley M, Haynes R. Assessment of tidal current energy in the Minas Passage, Bay of Fundy. Proceedings of the Institution of Mechanical Engineers, Part A: Journal of Power and Energy 2008;222(5):493–507.

[6] Brooks DA. The tidal-stream energy resource in passamaquoddy–Cobscook Bays: a fresh look at an old story. Renewable Energy 2006;31(14):2284–95.

[7] Brooks DA. The hydrokinetic power resource in a tidal estuary: The Kennebec River of the central maine coast. Renewable energy 2011;36(5):1492–501.

[8] Hasegawa D, Sheng J, Greenberg DA, Thompson KR. Far-field effects of tidal energy extraction in the Minas Passage on tidal circulation in the Bay of Fundy and Gulf of Maine using a nested-grid coastal circulation model. Ocean Dynamics 2011;61(11):1845–68.

[9] Pelling HE, Green M. Sea level rise and tidal power plants in the Gulf of Maine. Journal of Geophysical Research: Oceans 2013;118(6):2863–73.

[10] Karsten R, Swan A, Culina J. Assessment of arrays of in-stream tidal turbines in the Bay of Fundy. Phil Trans R Soc A 2013;371(1985):20120189.

[11] Copping A. The State of Knowledge for Environmental Effects Driving Consenting/Permitting for the Marine Renewable Energy Industry. Tech. Rep.; Ocean Energy Systems, International Energy Agency; 2018.

[12] Baring-Gould EI, Christol C, LiVecchi A, Kramer S, West A. A review of the environmental impacts for marine and hydrokinetic projects to inform regulatory permitting: Summary findings from the 2015 workshop on marine and hydrokinetic technologies, Washington, DC. Tech. Rep.; National Renewable Energy Lab.(NREL), Golden, CO (United States); 2016.

[13] Nash S, Phoenix A. A review of the current understanding of the hydro-

environmental impacts of energy removal by tidal turbines. Renewable and Sustainable Energy Reviews 2017;80:648–62.

[14] Neill SP, Jordan JR, Couch SJ. Impact of tidal energy converter (TEC) arrays on the dynamics of headland sand banks. Renewable Energy 2012;37(1):387–97.

[15] Sánchez M, Carballo R, Ramos V, Iglesias G. Tidal stream energy impact on the transient and residual flow in an estuary: a 3D analysis. Applied Energy 2014;116:167–77.

[16] Wu Y, Chaffey J, Greenberg DA, Smith PC. Environmental impacts caused by tidal power extraction in the upper Bay of Fundy. Atmosphere-Ocean 2016;54(3):326–36.

[17] Ashall LM, Mulligan RP, Law BA. Variability in suspended sediment concentration in the Minas Basin, Bay of Fundy, and implications for changes due to tidal power extraction. Coastal Engineering 2016;107:102–15.

[18] Chen C, Gao G, Qi J, Proshutinsky A, Beardsley RC, Kowalik Z, et al. A new high-resolution unstructured grid finite volume arctic ocean model (AO-FVCOM): An application for tidal studies. Journal of Geophysical Research: Oceans 2009;114(C8).

[19] Van Goor M, Zitman T, Wang Z, Stive M. Impact of sea-level rise on the morphological equilibrium state of tidal inlets. Marine Geology 2003;202(3-4):211–27.

[20] Scott DB, Greenberg DA. Relative sea-level rise and tidal development in the Fundy tidal system. Canadian Journal of Earth Sciences 1983;20(10):1554–64.

[21] Pelling H, Green M, Ward SL. Modelling tides and sea-level rise: To flood or not to flood. Ocean Modelling 2013;63:21–9.

[22] Pugh D, Woodworth P. Sea-Level Science: Understanding Tides, Surges, Tsunamis and Mean Sea-Level Changes. Früher erschienen u.d.T.: Pugh, David: Tides, tsunamis and mean sea-level changed; Cambridge University Press; 2014. ISBN 9781107028197. URL: https://books.google.com/books?id=QiBGAwAAQBAJ.

[23] Nicholls RJ, Cazenave A. Sea-level rise and its impact on coastal zones. science 2010;328(5985):1517–20.

[24] Wilmes SB. The impact of large-scale sea-level changes on tides in the past, present and future. Ph.D. thesis; School of Ocean Sciences Bangor University; 2016.

[25] Wilmes SB, Green J, Gomez N, Rippeth TP, Lau H. Global tidal impacts of large-scale ice sheet collapses. Journal of Geophysical Research: Oceans 2017;122(11):8354–70.

[26] Chen WB, Liu WC. Assessing the influence of sea level rise on tidal power output and tidal energy dissipation near a channel. Renewable Energy 2017;101:603–16.

[27] Tang H, Kraatz S, Qu K, Chen G, Aboobaker N, Jiang C. High-resolution survey of tidal energy towards power generation and influence

of sea-level-rise: A case study at coast of New Jersey, USA. Renewable and Sustainable Energy Reviews 2014;32:960–82.

[28] Shchepetkin AF, McWilliams JC. The regional oceanic modeling system (ROMS): a split-explicit, free-surface, topography-following-coordinate oceanic model. Ocean modelling 2005;9(4):347–404.

[29] Multon B. Marine Renewable Energy Handbook. ISTE; Wiley; 2013. ISBN 9781118603291. URL: https://books.google.com/books?id=yv6cYlKjk5cC.

[30] Hagerman G, Bedard R. Massachusetts tidal in-stream energy conversion (TISEC): survey and characterization of potential project sites. Electrical Power Research Institute EPRI-TP-003 MA Rev 2006;1.

[31] Cornett A, Durand N, Serrer M. 3-D Modelling and assessment of tidal current resources in the Bay of Fundy, Canada. 2010.

[32] Desplanque C, Mossman DJ. Bay of Fundy tides. Geoscience Canada 2001;28(1).

[33] Proudman J. Dynamical oceanography. Tech. Rep.; Methuen;; 1953.

[34] Neill SP, Hashemi MR, Lewis MJ. The role of tidal asymmetry in characterizing the tidal energy resource of Orkney. Renewable Energy 2014;68:337–50.

[35] Wang X, Chao Y, Dong C, Farrara J, Li Z, McWilliams JC, et al. Modeling tides in Monterey Bay, California. Deep Sea Research Part II: Topical Studies in Oceanography 2009;56(3-5):219–31.

[36] Ramos V, Carballo R, Álvarez M, Sánchez M, Iglesias G. Assessment of the impacts of tidal stream energy through high-resolution numerical modeling. Energy 2013;61:541–54.

[37] Debreu L, Marchesiello P, Penven P, Cambon G. Two-way nesting in split-explicit ocean models: algorithms, implementation and validation. Ocean Modelling 2012;49:1–21.

[38] Penven P, Debreu L, Marchesiello P, McWilliams JC. Evaluation and application of the roms 1-way embedding procedure to the central California upwelling system. Ocean Modelling 2006;12(1-2):157–87.

[39] Warner JC, Defne Z, Haas K, Arango HG. A wetting and drying scheme for roms. Computers & geosciences 2013;58:54–61.

[40] Haidvogel DB, Arango H, Budgell WP, Cornuelle BD, Curchitser E, Di Lorenzo E, et al. Ocean forecasting in terrain-following coordinates: Formulation and skill assessment of the regional ocean modeling system. Journal of Computational Physics 2008;227(7):3595–624.

[41] Warner JC, Sherwood CR, Arango HG, Signell RP. Performance of four turbulence closure models implemented using a generic length scale method. Ocean Modelling 2005;8(1):81–113.

[42] Egbert GD, Erofeeva SY. Efficient inverse modeling of barotropic ocean tides. Journal of Atmospheric and Oceanic Technology 2002;19(2):183–204.

[43] Garrett C, Cummins P. The efficiency of a turbine in a tidal channel. Journal of fluid mechanics 2007;588:243–51.

[44] Sutherland G, Foreman M, Garrett C. Tidal current energy assessment for Johnstone strait, Vancouver island. Proceedings of the Institution of Mechanical Engineers, Part A: Journal of Power and Energy 2007;221(2):147–57.

[45] Roc T, Conley DC, Greaves D. Methodology for tidal turbine representation in ocean circulation model. Renewable Energy 2013;51:448–64.

[46] Brown AJG, Neill SP, Lewis MJ. Tidal energy extraction in three-dimensional ocean models. Renewable Energy 2017;.

[47] International Electrotechnical Commission (IEC) . Marine energy - wave, tidal and other water current converters - part 201: Tidal energy resource assessment and characterization. IEC TS 2015;:62600 – 201.

[48] Pawlowicz R, Beardsley B, Lentz S. Classical tidal harmonic analysis including error estimates in MATLAB using t_tide. Computers & Geosciences 2002;28(8):929–37.

[49] Sucsy PV, Pearce BR, Panchang VG. Comparison of two-and three-dimensional model simulation of the effect of a tidal barrier on the Gulf of Maine tides. Journal of Physical Oceanography 1993;23(6):1231–48.

[50] Dupont F, Hannah CG, Greenberg D. Modelling the sea level of the upper Bay of Fundy. Atmosphere-Ocean 2005;43(1):33–47.

[51] Wu Y, Chaffey J, Greenberg DA, Colbo K, Smith PC. Tidally-induced sediment transport patterns in the upper Bay of Fundy: a numerical study. Continental Shelf Research 2011;31(19):2041–53.

[52] Pingree R, Griffiths D. Sand transport paths around the British Isles resulting from M2 and M4 tidal interactions. Journal of the Marine Biological Association of the United Kingdom 1979;59(2):497–513.

[53] Neill SP, Hashemi MR. Fundamentals of Ocean Renewable Energy: Generating Electricity from the Sea. Academic Press; 2018. ISBN 9780128104484.

[54] Myers L, Bahaj A. Simulated electrical power potential harnessed by marine current turbine arrays in the Alderney Race. Renewable energy 2005;30(11):1713–31.

[55] Zhou Z, Benbouzid M, Charpentier JF, Scuiller F, Tang T. Developments in large marine current turbine technologies–a review. Renewable and Sustainable Energy Reviews 2017;71:852–8.

[56] Sweet WV, Kopp RE, Weaver CP, Obeysekera J, Horton RM, Thieler ER, et al. Global and regional sea level rise scenarios for the United States. Tech. Rep.; NASA; 2017.

[57] MacEnri J, Reed M, Thiringer T. Power quality performance of the tidal energy converter, seagen. In: ASME 2011 30th International Conference on Ocean, Offshore and Arctic Engineering. American Society of Mechanical Engineers; 2011, p. 529–36.

[58] Musa M, Hill C, Sotiropoulos F, Guala M. Performance and resilience of hydrokinetic turbine arrays under large migrating fluvial bedforms. Nature Energy 2018;3(10):839.

[59] Fairley I, Masters I, Karunarathna H. The cumulative impact of tidal stream turbine arrays on sediment transport in the pentland firth. Renewable Energy 2015;80:755–69.

[60] Greenberg DA, Blanchard W, Smith B, Barrow E. Climate change, mean sea level and high tides in the Bay of Fundy. Atmosphere-Ocean 2012;50(3):261–76.